K^+ PRODUCTION IN THE SYSTEM NI+NI AT AN INCIDENT ENERGY OF 1.93 AGeV

Dieter Best, FOPI collaboration

GSI
Planckstr. 1
D-64291 Darmstadt
Germany

INTRODUCTION

The investigation of K^+ production in heavy ion collisions is interesting for several reasons. Relativistic transport model calculations for nucleus nucleus collisions indicate, that the yield and spectra of kaons are very sensitive to the nuclear equation of state (EOS)[1]. Because of the relative weak K^+–nucleon interaction ($\approx$ 10 mb), the measurement of K^+ mesons from heavy–ion collisions has thus been considered a promising way to probe not only the dense matter formed in the initial stage of the collision, when kaons are most likely to be produced [2, 3], but also the kaon properties in dense nuclear matter. Kaons might be subject to medium modifications. According to RBUU calculations of G. Q. Li and C. M. Ko [4] the maximum density reached in a Ni+Ni collision at 1.93 AGeV beam energy is about 3. Furthermore, the K^+ mass grows less than 10%, the K^- mass is reduced by 50% in this density range. This change is driven by the kaon potential in nuclear matter which is density dependent and has its origin in explicit chiral symmetry breaking. Kaon directed sideward flow has been proposed as an additional and even more sensitive probe than the yield for determining the in medium kaon potential [5, 4]. In addition, the yield is influenced by multistep processes, the ratio K^+/π^+ might be a sensitiv probe for resonance contributions to kaon production [6]. These probes (among others) remain to be very interesting as one proceeds to higher energies (AGS, SPS, RHIC, LHC) as new physics questions become relevant, for example verifying the phase transition of hadronic matter to the quark gluon plasma [7].

Therefore the FOPI collaboration has investigated with their 4π–detector K^+ production the symmetric system ^{58}Ni+^{58}Ni at 3 different incident energies: 1.93, 1.45, and 1.06 AGeV. Results of the analysis of the kaon data at 1.93 AGeV as obtained from the Central Drift Chamber (CDC) together with the time–of–flight Barrel of the FOPI detector have been published already in [8, 9, 10]. In the following results of the

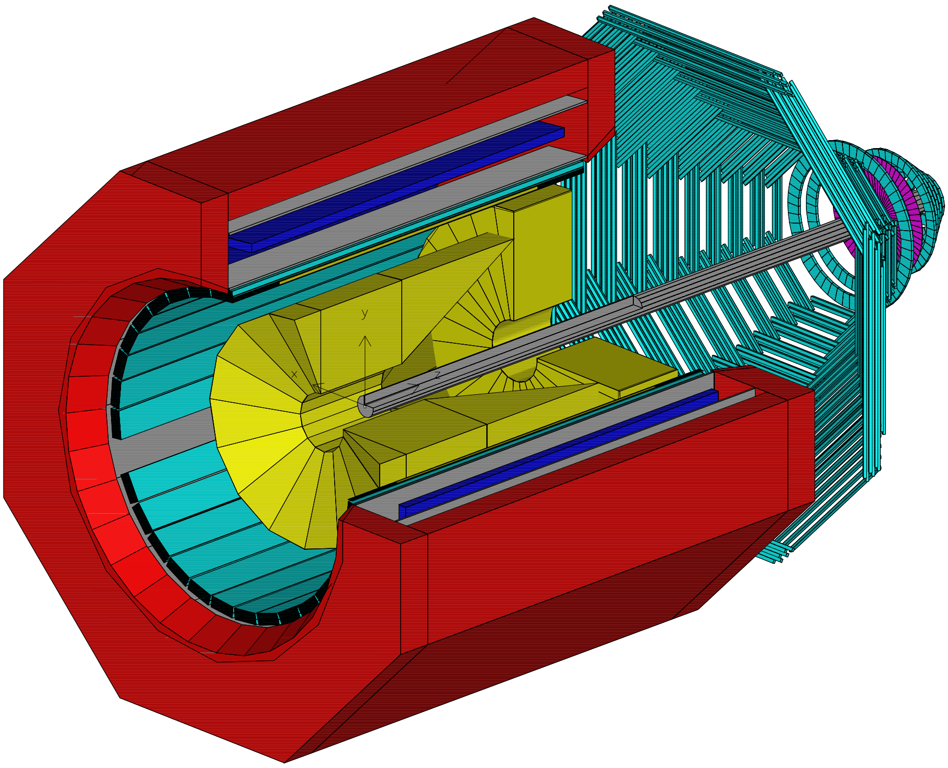

Figure 1. The FOPI detector at GSI.

analysis of $3{\cdot}10^6$ central events (innermost 10 % σ_{geo}) with respect to K^+ production at this beam energy are shown. After a short description of the experimental device and the method of particle identification transverse mass spectra and rapidity distributions are discussed. The results about the K^+/π^+ ratio are followed by the K^+ directed sideward flow analysis.

EXPERIMENTAL SETUP

The FOPI detector [11], shown in Figure 1, is a highly modular system of several subdetectors for fixed target experiments. It consists of 2 main parts with full azimuthal symmetry. One main component is the highly segmented Forward Plastic Wall which covers the polar angle between $1^o < \Theta_{Lab} < 30^o$ over the full azimuth. This setup is complemented by adding the Central Drift Chamber (CDC), a cylindrical tracking detector covering an additional range in polar angle of $30^0 < \Theta_{Lab} < 150^o$.

Pion, proton and deuteron identification is possible with the CDC alone using the Bethe–Bloch relation of the mean energy loss $< dE/dx >$ of a track with its momentum p. The high momentum limit of this method is overcome by adding the ToF information of the Barrel, thereby rising the particle identification capability. The chamber is surrounded by a ToF Plastic Barrel and a Cherenkov Barrel. Only a third of it has been installed during this experiment. The ToF resolution is about 1 ns FWHM, the covered polar angular range is $44^0 < \Theta_{Lab} < 160^o$.

The forward tracking chamber HELITRON will allow momentum measurements

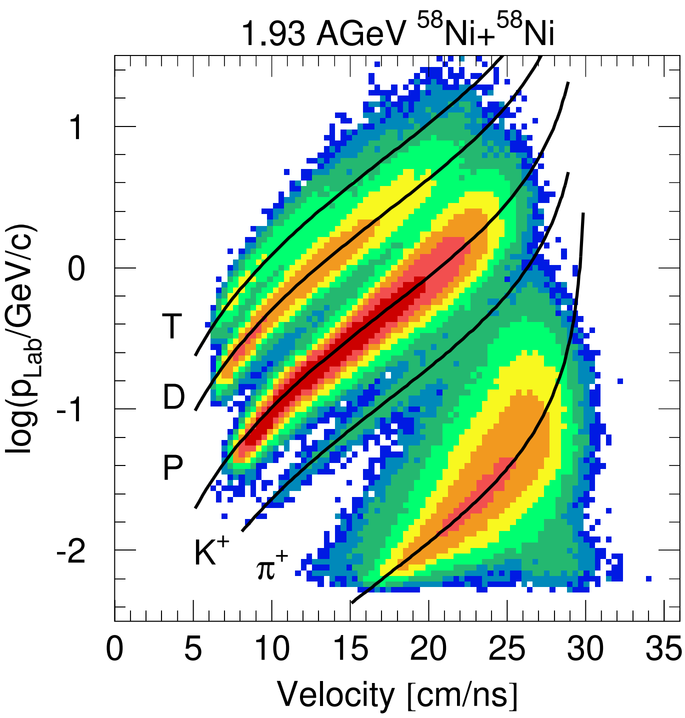

Figure 2. Momentum measured by the CDC plotted as function of velocity measured in the Barrel for particles with charge=+1.

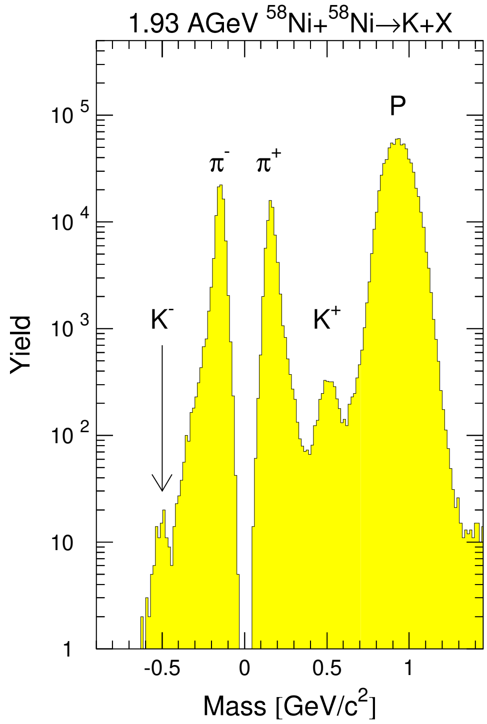

Figure 3. Reconstructed mass × charge using the matched CDC–Barrel data with $p_{Lab} < 500$ MeV/c for positively and negatively charged particles.

down to $\Theta_{Lab} \approx 7^o$. This detector was not yet installed during the experiment reported on here, but has been successfully employed in subsequent measurements.

The tracking chambers as well as the Barrel operate inside a magnetic field of about 0.6 T from a superconducting solenoid which allows the momentum determination for charged particles.

PARTICLE IDENTIFICATION

In order to enhance the particle identification capabilities of the CDC, the tracks are extrapolated to the Barrel detector and combined with the appropriate Barrel hit. The direct measurement of the time–of–flight t with the Scintillator Barrel allows to calculate the particle velocity from the path length L measured with the CDC: $\beta = L/ct$.

By combining the momentum p_{Lab} from the Central Drift Chamber (CDC) with the velocity information of the Barrel Figure 2 is obtained. Only positively charged particles are shown. Pions, protons, deuterons, and tritons are clearly resolved over the full velocity range. In addition a line between the pions and the protons is visible which is attributed to K^+ particles.

An additional mass value is obtained from the following formula:

$$mc^2 = pc \cdot \sqrt{\frac{1}{\beta^2} - 1}.$$

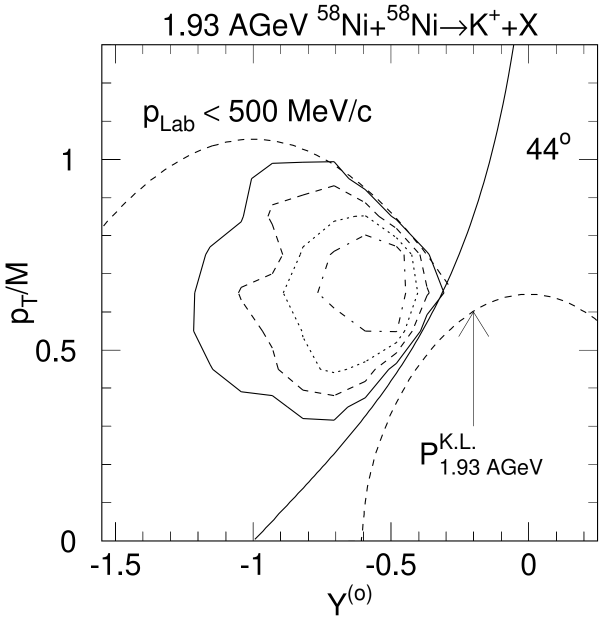

Figure 4. Transverse momentum p_T versus scaled rapidity $Y^{(0)}=Y/Y_{CM}$-1 for K^+ particles measured in Ni+Ni collisions at 1.93 AGeV.

After an upper limit of p_{Lab} <500 MeV/c has been applied in order to suppress protons and pions, a mass spectrum is obtained as shown in Figure 3. On the right hand side, between a peak at the π^+ mass and a much more pronounced proton peak another structure is clearly visible at the kaon mass of 494 MeV/c^2. Negatively charged particles have been plotted with a negativ mass for this display. Besides the π^- peak another statistically significant peak is visible which can be attributed to the K^-. The analysis of $3{\cdot}10^6$ central trigger events results in about 3000 K^+ mesons and about 30 K^- mesons within the Barrel acceptance which is about 4% of 4π. This results in a tentative background corrected ratio K^-/K^+ of about 1%. This is compatible with theoretical predictions of 2% [12] and earlier measurements at the BEVALAC [13]. However, further investigations are necessary to put this result on a firmer ground.

The strength of the FOPI detector, however, is the ability to measure a large area of phase space. In Figure 4 transverse momentum p_T/m versus scaled rapidity $Y^{(0)}=Y/Y_{CM}$-1 is shown for K^+ mesons. Target rapidity is at -1, midrapidity at 0 in this representation. Figure 4 is influenced by the acceptance of the Barrel which starts at a polar angle of 44^o. The upper momentum limit up to which K^+ particles can be identified is about 500 MeV/c at present. The lower transverse momentum limit is about 100 MeV/c, since the K^+ particles need this minimum p_T in order to reach the Barrel. The dashed line around midrapidity shows the kinematical limit for K^+ production in free pp collisions. Although the beam energy of 1.93 AGeV is above the free production threshold of 1.56 GeV it turns out that at least Fermi momentum is needed in order to produce K^+ mesons in the measured area.

TRANSVERSE MASS SPECTRA

Decay corrected multiplicities per unit of rapidity and transverse momentum, d^2N/dp_TdY, for positive kaons have been obtained as shown in Figure 5. The measurement extends from $p_T \approx 0.1\ GeV/c$ to $p_T \approx 0.5\ GeV/c$. Since the CDC–Barrel matching was involved in the K^+ analysis mostly target rapidities are measured. Details about the FOPI K^+ acceptance are described in [14, 8]. The differential multiplicity

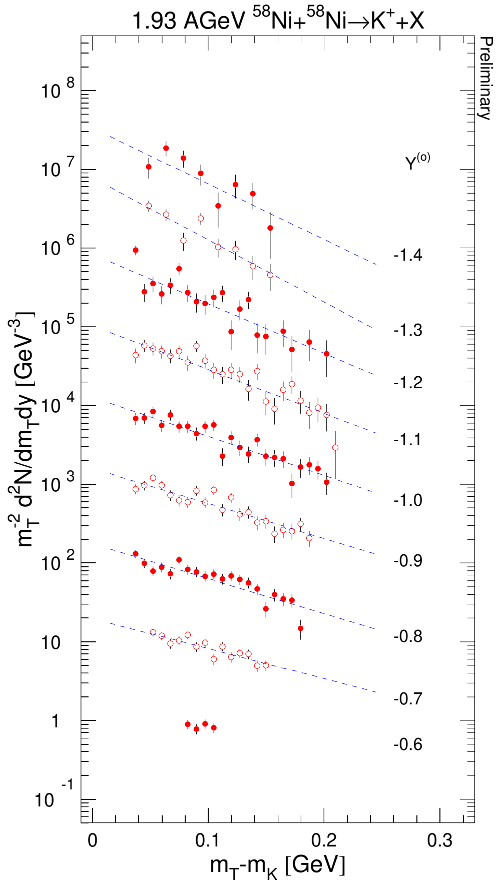

Figure 5. Measured K$^+$ m_T spectra for various slices in normalized rapidity.

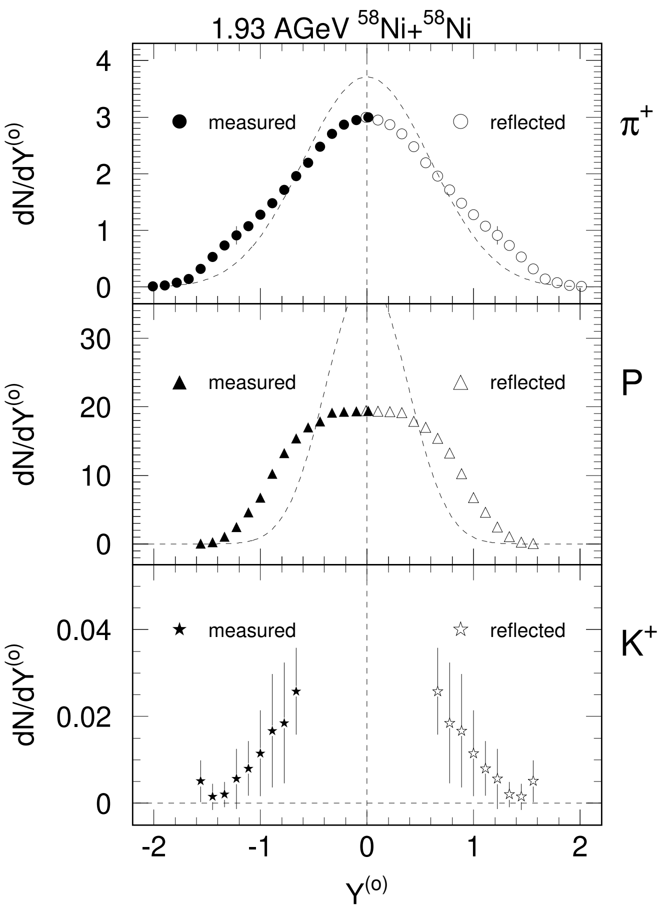

Figure 6. Measured yields of K$^+$, proton and π^+ as functions of normalized rapidity.

distribution is defined as

$$d^2N/dp^3 = m_T^{-2} d^2N/dm_T dY \tag{2}$$

where the quantity m_T is the transverse mass $m_T = \sqrt{p_T^2 + m^2}$. This parameterization has the advantage that a purely thermal Boltzmann model predicts that the number d^3N of particles of a given species in an element of phase space d^3p satisfies

$$\frac{d^3N}{d^3p} \propto \exp(-\frac{E}{T}),$$

where T is the temperature of the source and E the CM energy associated with d^3p. Figures 5 shows the resulting spectra in units of GeV^{-3} (c=1) versus $(m_T - m_o)$ for positive kaons and the central trigger condition in several rapidity slices. The lowest spectrum corresponds to the highest rapidity value.

Protons and charged pions are identified with the CDC alone. Details about the particle identification procedure and the corresponding acceptance investigations are found in [15].

Within the detector acceptance and the statistical fluctuations, the spectra for K$^+$ mesons, π^+, and protons seem to be described by an exponential function, as can be seen from the Figures [15]. Consequently, an exponential function

$$A \cdot \exp(-(m_T - m_o)/T_B),$$

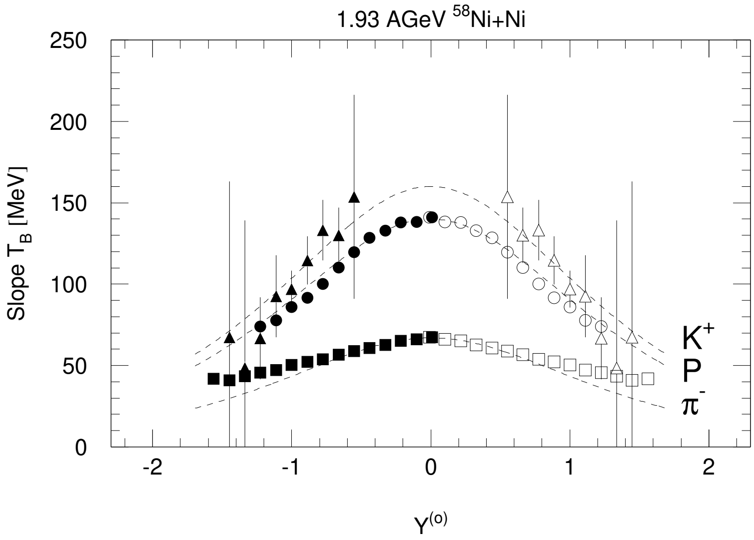

Figure 7. Measured slope parameter of K^+, proton and π^- as function of normalized rapidity.

where T is called the inverse slope parameter and A is the $p_T = 0$ intercept of the function at rapidity Y, has been fit to each spectrum. These fits, represented by the dashed lines in Figure 5, were performed by the maximum likelihood procedure for Poisson statistics.

It is very interesting to compare the apparent slopes of K^+, pions, and protons. This is shown in Figure 7. The Boltzmann slope parameters T_B in MeV are plotted as they are fitted for different rapidity slices. This is done for the π^-, protons and K^+. Whereas we have an upper momentum limit for the π^+ mesons of about p_{Lab} <600 MeV/c, we do not have this restriction for the identification of π^- mesons, which show a second hotter slope in the spectra beyond p_{Lab} ≈600 MeV/c. However, for comparison the π^- spectra have been fitted with one exponential only, which fits due to statistics reasons essentially the colder low momentum part. The black symbols in Figure 7 indicate the measured range, the open symbols are the reflected symbols around midrapidity. For a symmetric system like Ni+Ni forward and backward rapidities have to be the same. For an isotropic source T_B depends on rapidity according to this relation:

$$T_B = T/cosh(Y^{(0)}). \qquad (3)$$

The apparent slope T at midrapidity is

- 65 MeV for the π^- (single slope fit),
- 140 MeV for the protons,
- 160 MeV for the K^+ has to be estimated, since midrapidity is not reached with the Barrel detector.

This function is plotted as a dashed curve for all 3 particle species. The proton distribution is compatible with an isotropic source at midrapidity, whereas the pion distribution appears to be flatter. The distribution of K^+ mesons is compatible with an isotropic source. Most interestingly, however, the K^+ slopes seem to be at least in the order of the proton slopes. Schnetzer and collaborators have measured this relation already for Ne+NaF at 2.1 AGeV beam energy at the BEVALAC [16].

This is very interesting since depending on the ansatz one has different conclusions for the relation between the slopes of the different particle species. For example, if the

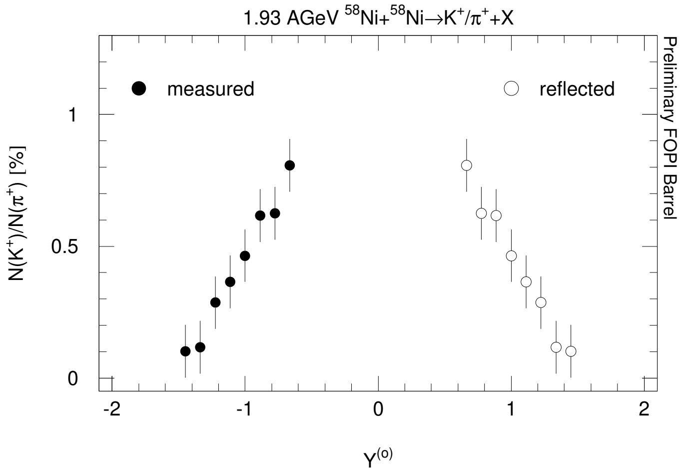

Figure 8. Ratio K^+/π^+ as function of scaled rapidity $Y^{(o)}$.

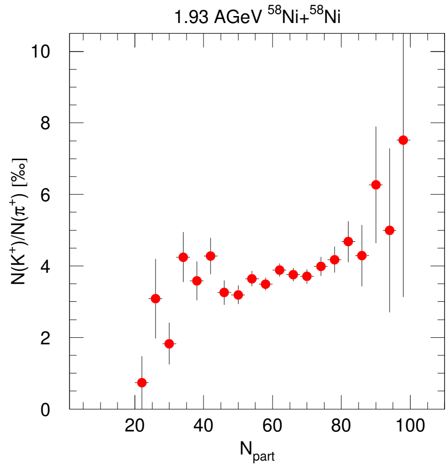

Figure 9. Ratio K^+/π^+ as function of number of participants.

dominating contribution would be radial flow, then the slopes would reflect the mass scaling of the different particle species [17]. This is not the case in our experiment. According to calculations scattering of kaons makes the spectra hotter [1]. The result shown in Figure 7 speaks in favour of a considerable amount of scattering for positively charged kaons. G. Q. Li and C. M. Ko found on the average 2 scatterings in their RBUU model for the symmetric system Ni+Ni at an incident energy of 1.93 AGeV and an impact parameter b=2 fm [12].

The systematic error on the inverse slope parameter T is $\approx 10\%$. It should be emphasized that the value of the inverse slope parameter T may in addition depend on the range $(m_T - m_\circ)$ used in the fitting procedure. This effect is not included in the systematic error estimates.

RAPIDITY DISTRIBUTIONS

The final multiplicity density, dN/dy, is obtained by integration, from $(m_T - m_\circ) = 0$ to $(m_T - m_\circ) = \infty$, of the exponential function and can be written as

$$\frac{dN}{dY} \propto A \cdot exp(-\frac{1}{k}) \cdot (2 + \frac{2}{k} + \frac{1}{k^2}) \cdot T^3 \qquad (4)$$

with $k=T/m_\circ$. The error for dN/dY (standard deviation) is evaluated from the deviation of the right term of the formula 4 using the variances and covariances of A and T. Figure 6 shows the rapidity distributions of positive pions, protons and K^+ mesons. The spectra with black symbols represent the measured values, the open symbols are reflected around midrapidity. The dashed lines represent the thermal model prediction using the apparent temperatures at midrapidity mentioned above. The total yield is adjusted to give the same result as the data. One point of note is the clearly nonthermal behaviour of the rapidity distributions for pions and protons.

K^+/π^+ RATIO

Dividing the dN/dy spectra of K^+ and π^+ the ratio K^+/π^+ is obtained as function of scaled rapidity $Y^{(o)}$ as shown in Figure 8. Since this result has been obtained within

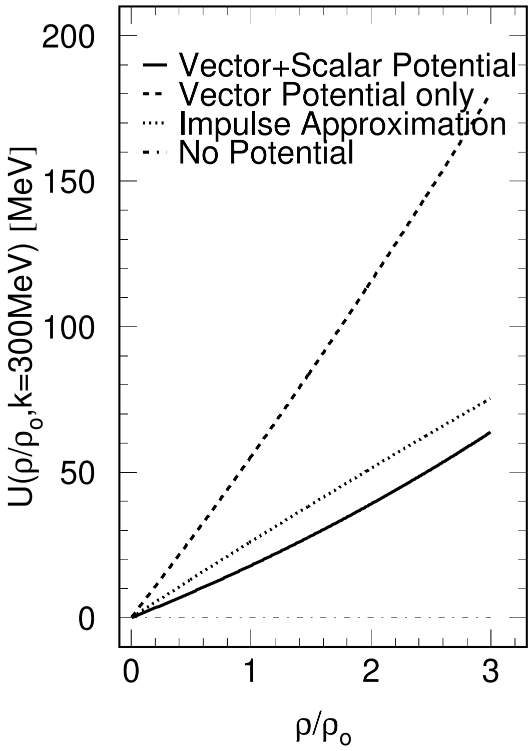

Figure 10. Dependence of K$^+$ in medium potential U on the normalized density ρ/ρ_o in the RBUU model of G. Q. Li and C. M. Ko. The results are shown for fixed K$^+$ momentum of 300 MeV/c.

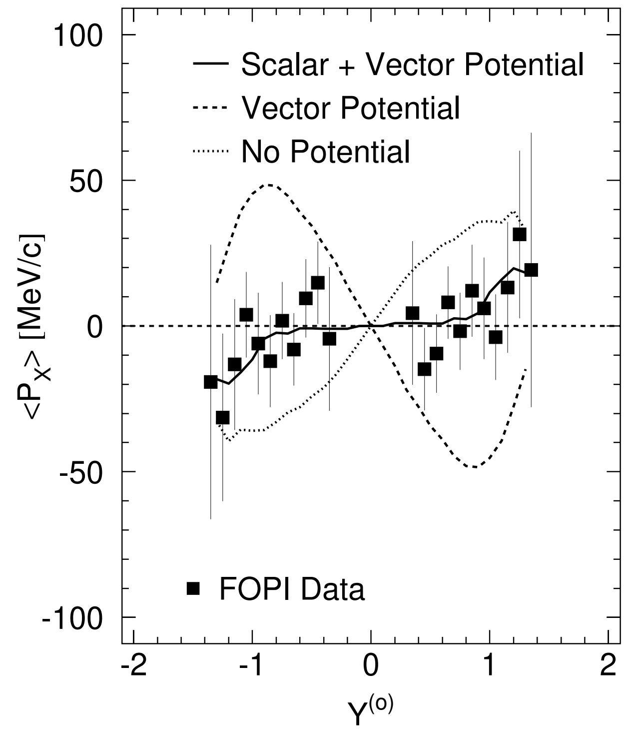

Figure 11. Measured transverse in–plane K$^+$ flow for ^{58}Ni+^{58}Ni at 1.93 AGeV. The results of calculations by G. Q. Li and C. M. Ko for different in medium kaon potentials are also given.

the Barrel acceptance midrapidity $Y^{(o)}=0$ is not reached. The ratio is on the 10^{-3} level and K$^+$ production is enhanced with respect to π^+ production as one approaches midrapidity.

Figure 9 shows this ratio in the Barrel acceptance as function of centrality. The ratio is at about 0.4 % and increases by 30% as the number of participants is increased by a factor of 2 from 40 to 80. However, since the acceptances of K$^+$ and π^+ mesons are different more subtle processes could play a role which makes further investigations necessary. This observable has been studied already intensively by the KaoS–Collaboration at GSI [6] for the symmetric system Au+Au at a beam energy of 1 AGeV. Their results at midrapidity show a rise of this ratio which has been interpreted as an indication that multistep processes play an important role for the quantitative explanation of K$^+$ yields at subthreshold energies.

Tentative comparisons with an RBUU model of C. M. Ko and G. Q. Li show that the K$^+$ enhancement of 30% for more central Ni+Ni collisions speaks in favour of an only moderate contribution of Δ resonances to the K$^+$ production, less than 25%, most of the kaons are produced in direct NN collisions, $\Delta\Delta$ collisions less than 5%. Higher resonances like N* are not included in the model [12].

DIRECTED SIDEWARD FLOW OF K$^+$

Not only do the spectra contain detailed information about kaon propagation properties during expansion they are also in particular sensitive to production processes.

In contrast to this kaon directed sideward flow is predicted to be a sensitive probe for kaon propagation properties during the expansion stage of a heavy ion collision [5, 4]. In order to measure kaon directed sideward flow a standard transverse momentum analysis according to Danielewicz and Odyniec [18] has been applied to the kaon data. The data shown in the following have been corrected for the variation of the reaction plane, which results in an increase of the flow signal by 30%.

In their RBUU model G. Q. Li and C. M. Ko start out with a chiral lagrangian which contains QCD motivated scalar and vector interactions of kaons with the surrounding baryonic matter. This results in a scalar and vector potential for the kaons. In Figure 10 the potential of positively charged kaons inside nuclear matter for fixed kaon momentum, 300 MeV/c, is plotted as function of normalized density ρ/ρ_o. Four possibilities have been investigated by the authors:

1. **no potential**: The kaons have no potential, they are treated as free particles, only the 10 mb elastic scattering is taken into account.
2. **vector potential**: Kaons have only a vector potential, which is strongly repulsive.
3. **vector and scalar potential**: Kaons have in addition to the vector potential a scalar potential. The scalar potential is attractive, therefore the resulting potential is far less repulsive.
4. **impulse approximation**: The impulse approximation is a repulsive potential which has been obtained as a result of a fit to kaon–nucleon scattering data. The degree of repulsion is smaller than for the vector potential but stronger than for the scalar plus vector potential.

In all these situations the total effective potential is repulsive. Figure 11 shows the model results for the symmetric system Ni+Ni at an incident beam energy of 1.93 AGeV and an impact parameter range of b<4 fm. An upper limit in transverse momentum of p_T >250 MeV/c is applied to the model results in order to cope with the FOPI kaon acceptance. Depending on the potential used in the model, the kaon flow behaviour is very different:

1. **no potential**: For the no potential option kaons flow like protons, but with a smaller flow velocity. At target rapidity $< p_X >$ is about -40 MeV.
2. **vector potential**: For the vector potential option kaons show an antiflow, since the vector potential is strongly repulsive, about 50 MeV at target rapidity.
3. **vector and scalar potential**: In this case with both scalar and vector potentials, kaons show no flow signal.
4. **impulse approximation**: The impulse approximation is indistinguishable with the scalar plus vector potential option on this level.

In comparison the data are shown as black squares and although error bars are still large, the trend is obvious, the data seem to favour the option with scalar and vector potential. Since mostly target rapidities are measured for the K^+ mesons the data have been symmetrized around midrapidity in order to get a more complete picture.

The remaining ambiguity between impulse approximation and scalar+vector option can be resolved by using additional information, e.g. investigating impact parameter dependencies. Another possibility is the K^-/K^+ ratio which should be greater for impulse approximation [19].

SUMMARY AND OUTLOOK

In summary we have shown the successful identification of K mesons over a wider range of rapidities for this system and energy range for the first time. Besides the remarkable observation that the Boltzmann slopes of the kaon m_T spectra are at least in the order of the proton slopes, we have measured a rising ratio K^+/π^+ with centrality. Directed sideward flow for K^+ mesons has been measured for the first time. In this way it was possible to extend earlier measurements and to address the question of the kaon in medium potential and therefore in medium effects on kaons. The data seem to favour a combined scalar and vector potential. However there remains an ambiguity between this potential and the impulse approximation which is distinguishable by using additional information.

Recently FOPI has measured an additional $7 \cdot 10^6$ central events for the symmetric system Ni+Ni at an incident energy of 1.93 AGeV which results in an order of magnitude higher statistics for kaons. This will enable us to investigate the centrality dependence of the above mentioned kaon observables and in particular to solve the ambiguity in the explanation of the kaon flow data mentioned above. The use of additional observables as $dN/d\phi$ [20] or K^-/K^+ could shed more light on this issue. Future analysis will exploit the unique possibilities of the FOPI 4π detector to supply many observables which competing models have to fit simultaneously as has been tried in [21].

ACKNOWLEDGMENTS

The author wants to thank the organizers of this workshop for the invitation, P. Braun–Munzinger, the colleagues N. Herrmann, J. Ritman, B. Hong and M. Kirejczyk, and the theorists G. Brown, V. Koch, G. Q. Li, B. A. Li, M. Prakash and H. Sorge for useful discussions.

REFERENCES

1. C. Hartnack et al., Nucl. Phys. 580 (1994) 643–677.
2. J. Randrup and C. M. Ko, Nucl. Phys. A 343 (1980) 519, Nucl. Phys. A 411 (1981) 537.
3. J. Aichelin and C. M. Ko, Phys. Rev. Lett. 55 (1985) 2661.
4. G. Q. Li and C. M. Ko, Nucl. Phys. A 594 (1995) 460–482.
5. G. Q. Li, C. M. Ko and B. A. Li, Phys. Rev. Lett. 74 (1995) 235.
6. D. Miskowiec et al., Phys. Rev. Lett. 72 (1994) 3650.
7. J. W. Harris and B. Müller, The Search for the Quark–Gluon Plasma, hep-ph/9602235.
8. D. Best, Proceedings Bormio, 1995, p.505.
9. J. L. Ritman, Proceedings Hirschegg, 1995, p.340.
10. J. L. Ritman et al., Z. Phys. A 352 (1995) 355–357.
11. A. Gobbi et al., Nucl. Inst. Meth. 324 (1993) 156–176.
12. G. Q. Li, private communication.
13. A. Shor et al., Phys. Rev. Lett. 48 (1982) 1595, Phys. Rev. Lett. 63 (1989) 2192.
14. D. Best, GSI Scientific Report 1994, p.84.
15. D. Best, Ph.D. thesis, Heidelberg, 1996.
16. S. Schnetzer et al., Phys. Rev. Lett. 49 (1982) 989, Phys. Rev. C 40 (1989) 640.
17. P. Siemens and J. O. Rasmussen, Phys. Rev. Lett. 42 (1979) 880.
18. P. Danielewicz and G. Odyniec, Phys. Lett. B 157 (1985) 146.
19. C. M. Ko, Proceedings Hirschegg, 1995, p.192.
20. G. Q. Li, C. M. Ko, and G. E. Brown, Phys. Lett. B, submitted
21. G. E. Brown, C. M. Ko, and G. Q. Li, Nucl. Phys. A, submitted